ASCE JOURNAL OF AEROSPACE ENGINEERING

ISSN: 0893-1321 **eISSN:** 1943-5525

PUBLISHED ONLINE MARCH 15TH 2016

DOI: 10.1061/(ASCE)AS.1943-5525.0000614

MULTIPLE SLIP AND VARIABLE TRANSPORT PROPERTY EFFECTS ON MAGNETO-HYDROMAGNETIC DISSIPATIVE THERMO-SOLUTAL CONVECTION IN POROUS MEDIA

M.J. Uddin[1*], O.A. Bég[2], M.N Uddin[3]

ABSTRACT

A mathematical study is presented to investigate the influence of variable transport properties and momentum, thermal and mass slip on magnetohydrodynamic (MHD) momentum, heat and mass transfer in a porous media. Slip effects are simulated via careful imposition of boundary conditions at the wall. Joule heating and viscous dissipation are also studied. The governing partial differential boundary layer equations are analyzed using Lie group theory and rendered with appropriate transformations into a system of nonlinear, coupled ordinary differential equations. The multi-physical boundary value problem is dictated by twelve thermophysical parameters- concentration diffusivity parameter (Dc), Hartmann magnetic number (M), permeability parameter (Ω), Eckert number (Ec), momentum slip (a), thermal slip (b), mass (species) slip (d), Prandtl number (Pr), Schmidt number (Sc), power law index for non-isothermal and non-iso-solutal effects (m), viscosity variation parameter (A) and thermal conductivity variation parameter (S). A numerical solution is obtained for the effects of selected parameters on transport characteristics using the robust Runge-Kutta-Fehlberg fourth-fifth order numerical quadrature method in **Maple16**. Excellent correlation is achieved between the present computational results and for the constant transport properties ($A=S=Dc=0$), non-porous ($\Omega=0$), non-thermal slip (b=0), non-solutal slip ($d=0$) and non-dissipative solutions without Joule heating (Ec= 0) of Yazdi et al. [35]. Increasing momentum slip enhances temperatures whereas increasing thermal slip reduces them. An increase in thermal conductivity boosts temperatures whereas greater viscosity reduces temperatures. Increasing magnetic parameter suppresses velocity and increasing permeability parameter elevates temperatures. Species concentration is enhanced with increasing concentration diffusivity and permeability parameter but depressed with increasing viscosity. Furthermore concentration is enhanced with momentum slip but reduced with mass slip parameter. Moreover increasing magnetic field is observed to aid species diffusion in the regime. The present study finds applications in trickle-bed reactor hydromagnetics, magnetic polymeric materials processing and MHD energy generator slip flows.

Keywords: Slip; porous media, Lie group; heat and mass transfer; magnetic field; polymer processing; viscosity, thermal conductivity and mass diffusivity effects, **Maple16**

1. Corresponding author: Md. Jashim Uddin, Associate Professor of Mathematics, American International University-Bangladesh, Banani, Dhaka 1213, Bangladesh, Email: drjashim@aiub.edu, jashim_74@yahoo.com,
Tel: +60104625506
2. Spray Research Group, School of Computing, Science and Engineering, Newton Bldg, The Crescent, University of Salford, Manchester, M54WT, **England, UK**, U.K. E-mail: gortoab@gmail.com; O.A.Beg@salford.ac.uk
3. Department of Mathematical Sciences, Ball State University 2000 W University Avenue Muncie, IN 47306, USA.
Email:" muddin@bsu.edu

Nomenclature

a	the momentum slip parameter
B	magnetic field strength
C	concentration
C_w	wall concentration
C_∞	ambient concentration
$D(C)$	variable mass diffusivity
Dc	diffusivity parameter
D_m	diffusion coefficient (kg/m s)
Ec	Eckert number
$f(\eta)$	dimensionless stream function
f_w	mass transfer parameter
g	acceleration due to gravity (ms^{-2})
k	thermal conductivity (m^2s)
K	reaction parameter
k_1	Rosseland mean absorption coefficient
L	characteristic length (m)
m	power law index
M	magnetic field parameter
n	order of chemical reaction
N_1	velocity slip factor
$Nu_{\bar{x}}$	local Nusselt number

Pr Prandtl number

p pressure (Nm^{-2})

q_m wall mass flux ($kg/s\ m^2$)

q_r Radiative heat flux ($W/\ m^2$)

q_w wall heat flux ($W/\ m^2$)

R Radiation parameter

Sc Schmidt number

T nanofluid temperature (K)

T_w wall temperature (K)

T_∞ ambient temperature (K)

$\bar{u}, \bar{v}$ velocity components along $\bar{x}-$ and $\bar{y}-$axes (ms^{-1})

$\bar{x}, \bar{y}$ Cartesian coordinates along and normal to the axes (m)

Greek symbols

α thermal diffusivity of the porous medium ($m^2/\ s$)

μ viscosity of the base fluid (Ns/m^2)

Ω porosity parameter

ν kinematic viscosity of the fluid ($m^2/\ s$)

σ electric conductivity

σ_1 Stefan Boltzmann constant

$\phi(\eta)$ dimensionless concentration

η similarity independent variable

$\theta(\eta)$ dimensionless temperature

ρ fluid density (kg/m^3)

ψ stream function

Introduction

Magnetohydrodynamic flows in electrically-conducting fluids arise in many sophisticated applications in modern chemical engineering and materials processing. These include magnetic field control of heat and mass transfer [1-5], trickle bed reactor catalytic process intensification with magnetic fields [6-7], electromagnetic microwave combination heating [8], binary gas separation with magnetism [9], crystal growth fabrication [10] and magneto-thermal regulation of semi-conductor synthesis [11-121]. In many of these regimes both heat and mass transfer may occur simultaneously and fluids may have variable thermophysical properties e.g. viscosity, conductivity etc. Porous media may also feature in these applications as may viscous heating and Ohmic dissipation (Joule heating) effects. Many theoretical studies in this regard have been communicated utilizing a diverse range of numerical and analytical schemes. Zueco et al. [13] studied thermal conductivity and thermophoresis effects on magneto-convection using a network simulation method. They showed that thermal boundary layer thickness is increased significantly with increasing thermal conductivity. Mukhopadhyay and Layek [14] studied fluid viscosity variation effects on convection in heat generating porous media using a special form of Lie group transformations and a shooting method and found that horizontal velocity is depressed close to the wall with increasing temperature-dependent fluid viscosity parameter. Further studies of viscosity variation on transport phenomena have been communicated by Cortell [15] for radiative flows, Tripathi et al. [16] for biomimetic peristaltic pump flows, Acros et al. [17] for condensation flow, Mahmoud [18] for viscoelastic magneto-convection, Shateyi and Motsa [19] for Hall current magneto-gas dynamic flow (using a Chebyshev pseudospectral method) and Muhaimin et al. [20] for reactive double-diffusive convection. Further investigations of variable thermal conductivity effects have been reported by Bég et al. [21] who studied dissipative nonlinear heat transfer in porous media using a Keller box difference algorithm and Aziz and Lopez [22] who considered radiation flow from rods and sheets. Gorla and Hossain [23] very recently studied Joule heating and viscous dissipation effects on magnetic boundary layer flows. The importance of included viscous heating in non-isothermal chemical engineering flows (as studied in the present paper), has also been documented by Ybarra and Eckert [24].

The above studies have used the conventional "no-slip" boundary conditions. However many flow phenomena in chemical engineering require the consideration of *slip* at the boundary. Important applications in this regard are molten polymer capillary flows [25], metallocene-catalyzed bimodal polyethylene thermal hydrodynamics and rotating disk MHD generator flows [26]. Many approaches have been developed to simulate momentum (velocity slip) including the use of the Knudsen number and a wall slip parameter. Iliuta et al. [27] derived wall slip functions for trickle-flow reactors in terms of the dimensionless gas Reynolds, liquid Reynolds, Froude, Weber, Lockhart-Martinelli and Stokes numbers. Augier et al. [28] used particle image velocimetry (PIV) to study slip effects a vertical cocurrent flow of n-heptane dispersed in an aqueous solution of glycerin. Tripathi et al. [29] studied analytically with a homotopy method, the wall slip on viscoelastic propulsion in axisymmetric tube flows. Lok et al. [30] investigated numerically the steady boundary layer flow of a micropolar fluid near an oblique stagnation point on a fixed surface with Navier's slip condition.

In the context of heat and mass transfer, most investigations have been confined to the case of constant mass diffusivity. However, mass diffusivity has been shown to depend on the concentration of diffusing substance. Such concentration dependence exists in many process engineering systems, where the diffusion coefficient varies with the concentration over a certain range. The diffusion coefficient can often be approximated by a linear or exponential dependence equation as elaborated by Azuara [31], White and Subramanian [32] and Cussler [33]. Hamad et al. [34] studied the effect of variable mass diffusivity on the flow, heat and mass transfer. They found employing Lie group theory that mass diffusivity parameter enhances species concentration. Very recently, Uddin et al. [35] investigated the influence of slip and variable mass diffusivity on heat and mass transfer in a Darcy porous medium.

The aim of the present paper is to extend the work of Yazdi et al. [36] to simulate magnetized double-diffusive convection in porous media with the effects of the concentration dependent mass diffusivity, the temperature dependent viscosity and the thermal conductivity, and velocity slip, thermal slip and mass slip. Instead of using existing similarity transformations in the literature we generate them with a robust Lie group analysis and hence transform the governing partial differential transport equations to ordinary (similarity) differential equations. The resulting similarity equations are solved numerically with **Maple 16**. The influence of the thermo-physical controlling

parameters on the dimensionless velocity, temperature, and concentration distributions are elucidated. Furthermore the effects of the emerging parameters on surface shear stress function (friction factor), wall heat transfer rate (local Nusselt number) and wall mass transfer rate (local Sherwood number) are also studied in detail. The present simulations constitute a substantial extension to the existing work in the literature and have applications in magnetic materials processing [2].

Thermophysical magneto-fluid dynamics model

The two-dimensional steady magnetohydrodynamic (MHD) Newtonian laminar boundary layer flow of an electrically conducting fluid along a non-isothermal and non-isosolutal moving vertical surface embedded in a fluid-saturated porous medium is considered. The physical regime under investigation is depicted in **Fig.** 1. A variable transverse magnetic field $B(x)$ acts normal to the bounding surface. Viscous dissipation and Joule heating terms in the energy equation are incorporated. The wall temperature $T_w(x)$ is greater than the free stream temperature T_∞. The wall concentration $C_w(x)$ is also greater than the free stream concentration C_∞. Following Mukhopadhyay and Layek [14], we assume the temperature dependent viscosity varies according to $\mu = \mu_\infty\left[1+b_0\left(T_w - T\right)\right] = \mu_\infty\left[1+A\left(1-\theta\right)\right]$ where μ_∞ is the constant undisturbed viscosity b_0 is constant with $b_0 > 0$, $A = b_0(T_w - T_\infty)$ is the viscosity variation parameter. It is also assumed, following Aziz and Lopez [22], that thermal conductivity k obeys a linear temperature law according to $k = k_\infty\left[1+c_1(T-T_\infty)\right] = k_\infty\left[1+S\,\theta\right]$, where k_∞ is constant thermal conductivity, c_1 is a thermophysical constant dependent on the fluid; c_1 < 0 for lubrication oils, hydromagnetic working fluids and c_1 > 0 for air or water and $S = c_1(T_w - T_\infty)$ is the thermal conductivity variation parameter The range of variation of *S* can be taken as follows, for air $0 \le S \le 6$ for water $0 \le S \le 0.12$ and for lubrication oils $-0.1 \le S \le 0$ as elaborated by Cortell [15]. It is further assumed that mass diffusivity D obeys a linear concentration law according to $D = D_\infty\left[1+c(C-C_\infty)\right] = D_\infty\left[1+Dc\,\phi\right]$, where D_∞ is the constant mass diffusivity, c is constant and $Dc = c\,(C_w - C_\infty)$ is a concentration diffusivity parameter, following White and Subramanian [32]. In the diffusion of vapours in high-polymer substances, the concentration dependence is a very significant feature. We assume that concentration of the diffusing species is very low

thereby negating cross diffusion (Soret and Dufour effects). The magnetic Reynolds number is small so that the induced magnetic field is negligible in comparison to the applied magnetic field [13]. We neglect electric field associated with the polarization of charges and Hall effects. The governing boundary layer equations which are parabolic in nature, in dimensionless form are:

$$\frac{\partial \bar{u}}{\partial \bar{x}} + \frac{\partial \bar{v}}{\partial \bar{y}} = 0, \tag{1}$$

$$\bar{u}\frac{\partial \bar{u}}{\partial \bar{x}} + \bar{v}\frac{\partial \bar{u}}{\partial \bar{y}} = \frac{\mu(T)}{\rho_\infty}\frac{\partial^2 \bar{u}}{\partial \bar{y}^2} + \frac{1}{\rho_\infty}\frac{\partial \mu(T)}{\partial T}\frac{\partial T}{\partial \bar{y}}\frac{\partial \bar{u}}{\partial \bar{y}} - \frac{\mu(T)}{\rho_\infty K(\bar{x}/L)}\bar{u} - \frac{\sigma B^2(\bar{x}/L)}{\rho_\infty}\bar{u}, \tag{2}$$

$$\bar{u}\frac{\partial T}{\partial \bar{x}} + \bar{v}\frac{\partial T}{\partial \bar{y}} = \frac{1}{\rho_\infty c_p}\frac{\partial}{\partial \bar{y}}\left(k(T)\frac{\partial T}{\partial \bar{y}}\right) + \frac{\mu(T)}{\rho_\infty c_p}\left(\frac{\partial \bar{u}}{\partial \bar{y}}\right)^2 + \frac{\sigma B^2(\bar{x}/L)}{c_p \rho_\infty}\bar{u}^2, \tag{3}$$

$$\bar{u}\frac{\partial C}{\partial \bar{x}} + \bar{v}\frac{\partial C}{\partial \bar{y}} = \frac{\partial}{\partial \bar{y}}\left[D(C)\frac{\partial C}{\partial \bar{y}}\right]. \tag{4}$$

The boundary conditions at the surface and far from the vertical plate are, following Datta [37], Karniadakis et al. [38]:

$$\begin{aligned} &\bar{u} = \bar{u}_w + \bar{u}_{slip} = \left(\frac{\bar{x}}{L}\right)^m U_r + \frac{\mu(T)}{\rho_\infty}N_1\left(\frac{\bar{x}}{L}\right)\frac{\partial \bar{u}}{\partial \bar{y}}, \bar{v} = 0, T = T_w + D_1\left(\frac{\bar{x}}{L}\right)\frac{\partial T}{\partial \bar{y}}, \\ &C = C_w\left(\frac{\bar{x}}{L}\right) + + E_1\left(\frac{\bar{x}}{L}\right)\frac{\partial C}{\partial \bar{y}} \quad \text{at } \bar{y} = 0, \\ &\bar{u} \to 0, \ T \to T_\infty, \ C \to C_\infty \quad \text{as } \bar{y} \to \infty. \end{aligned} \tag{5}$$

Here the following notation applies $(\bar{u}, \bar{v})$: Darcian velocity components along axes, $\mu(T)$: variable dynamic coefficient of viscosity, $k(T)$: variable thermal conductivity, K: permeability of the porous media, ρ_∞: density of the fluid, σ: electric conductivity, c_p: specific heat at constant pressure, $D(C)$: variable mass diffusivity, $\bar{u}_w$: velocity of the plate, $N_1(\bar{x}/L)$: variable velocity slip factor, $D_1(\bar{x}/L)$: variable thermal slip factor, $E_1(\bar{x}/L)$: variable solutal slip factor. We assumed the form of the magnetic field, wall temperature and wall concentration as follows:

$$B(\bar{x}) = B_0\left(\bar{x}/L\right)^{\frac{m-1}{2}}, \ T_w(\bar{x}/L) = T_\infty + \left(\Delta T\right)_0\left(\bar{x}/L\right)^{2m}, C_w(\bar{x}/L) = C_\infty + \left(\Delta C\right)_0\left(\bar{x}/L\right)^{2m}, \tag{6}$$

where B_0, $\left(\Delta T\right)_0$, $\left(\Delta C\right)_0$ are constants and *m* is the power law index. Purely analytical solutions to the partial differential boundary value problem defined by Eqns. (1)-(5) are intractable. Even a numerical solution is complicated. Hence we aim to transform the problem to a system of ordinary differential equations.

Non-dimensionalizations of the transport equations

Proceeding with the analysis, we introduce the following dimensionless variables:

$$x=\frac{\bar{x}}{L},\ y=\frac{\bar{y}\sqrt{\mathrm{Re}}}{L},\ u=\frac{\bar{u}}{U_r},\ v=\frac{\bar{v}\sqrt{\mathrm{Re}}}{U_r},\ \theta=\frac{T-T_\infty}{T_w-T_\infty},\ \phi=\frac{C-C_\infty}{C_w-C_\infty} \tag{7}$$

with L being the characteristic length, U_r denoting a reference velocity and $\mathrm{Re}=\frac{U_r L\rho_\infty}{\mu_\infty}$ representing the Reynolds number. Furthermore we invoke a stream function ψ which satisfies the Cauchy-Riemann equations, $u=\frac{\partial\psi}{\partial y},\ v=-\frac{\partial\psi}{\partial x}$, Eqns. (2)-(4) reduce to:

$$\begin{aligned}&\frac{\partial\psi}{\partial y}\frac{\partial^2\psi}{\partial x\partial y}-\frac{\partial\psi}{\partial x}\frac{\partial^2\psi}{\partial y^2}=\left(1+A(1-\theta)\right)\frac{\partial^3\psi}{\partial y^3}\\&-A\frac{\partial^2\psi}{\partial y^2}\frac{\partial\theta}{\partial y}-M\,x^{m-1}\frac{\partial\psi}{\partial y}-\frac{\Omega}{g(x)}\left[1+A\left(1-\theta\right)\right]\frac{\partial\psi}{\partial y},\end{aligned} \tag{8}$$

$$\begin{aligned}&\frac{\partial\psi}{\partial y}\frac{\partial\theta}{\partial x}-\frac{\partial\psi}{\partial x}\frac{\partial\theta}{\partial y}+\frac{\partial\psi}{\partial y}\theta\frac{\partial}{\partial x}\left(\ln\Delta T\right)=\frac{1}{\mathrm{Pr}}\left[1+S\theta\right]\frac{\partial^2\theta}{\partial y^2}+\frac{1}{\mathrm{Pr}}S\left(\frac{\partial\theta}{\partial y}\right)^2\\&+\frac{Ec}{x^{2m}}\left[1+A\left(1-\theta\right)\right]\left(\frac{\partial^2\psi}{\partial y^2}\right)^2+\frac{Ec.M}{x^{1+m}}\left(\frac{\partial\psi}{\partial y}\right)^2,\end{aligned} \tag{9}$$

$$\frac{\partial\psi}{\partial y}\frac{\partial\phi}{\partial x}+\frac{\partial\psi}{\partial y}\phi\frac{\partial}{\partial x}\left(\ln\Delta C\right)-\frac{\partial\psi}{\partial x}\frac{\partial\phi}{\partial y}=\frac{1}{Sc}\frac{\partial}{\partial y}\left[(1+Dc\,\phi)\ \frac{\partial\phi}{\partial y}\right]. \tag{10}$$

The boundary conditions in Eqn. (5) can be shown to reduce to:

$$\begin{aligned}&\frac{\partial\psi}{\partial y}=x^m+a\,l_1(x)\left[1+A\left(1-\theta\right)\right]\frac{\partial^2\psi}{\partial y^2},\ \frac{\partial\psi}{\partial x}=0,\ \ \theta=1+b\,l_2(x)\frac{\partial\theta}{\partial y},\\&\phi=1+d\,l_3(x)\ \frac{\partial\phi}{\partial y}\ \text{at}\quad y=0,\\&\frac{\partial\psi}{\partial y}\to 0,\ \theta\to 0,\ \phi\to 0\quad\text{as}\quad y\to\infty.\end{aligned} \tag{11}$$

The parameters in Eqns. (8)-(11) are defined as follows: $M=\sigma B_0^2 L/\rho_\infty U_r$ (magnetic field parameter i.e. square of the Hartmann number), $\Omega=\mu_\infty/\rho_\infty K_0 U_r$ (inverse permeability parameter), $Ec=U_r^2/c_p\left(\Delta T\right)_0$ (Eckert number), $a=\left(N_1\right)_0\mu_\infty\sqrt{\mathrm{Re}}/\rho_\infty L$ (velocity slip), $b=\left(D_1\right)_0\sqrt{\mathrm{Re}}/L$ (thermal slip), $d=\left(E_1\right)_0\sqrt{\mathrm{Re}}/L$ (mass slip), $\mathrm{Pr}=\mu_\infty c_p/k_\infty$ (Prandtl number), $Sc=\nu_\infty/D_\infty$ (Schmidt number). Inspection of Eqn. (9)

shows that Ec also appears in the final term on the right hand side i.e. the Joule heating term (also known as Ohmic dissipation, this is the heating effect generated by the magnetic field). In the case of low speed incompressible flows (as consider in this paper), Ec represents the difference between the total mechanical power input and the smaller amount of total power input which produces thermodynamically reversible effects, i.e. elevations in kinetic and potential energy. This difference constitutes the energy dissipated as thermal energy by viscous effects, i.e. work done by the viscous fluid in overcoming internal friction, hence the term viscous heating. We note that $Ec > 0$ corresponds to the wall cooling scenario i.e., loss of heat from the wall to the fluid; $Ec < 0$ implies the wall heating scenario i.e. heat received by the wall from the fluid. We focus on the former case. In the above analysis, it has been It was assumed that

$$K(x) = K_0\, g(x), \qquad N_1(x) = (N_1)_0\, l_1(x), \qquad D_1(x) = (D_1)_o\ l_2(x), \quad E(x) = (E_1)_0\ l_3(x)$$

where $K_0, (N_1)_0$, $(D_1)_0$ and $(E_1)_0$ are constant permeability, hydrodynamic slip, thermal slip and solutal slip. Subsequently we develop invariant transformations which will convert the partial differential equations as well as the boundary conditions from two independent variables $(\bar{x}, \bar{y})$ to a system of non-linear ordinary differential equations in a single independent spatial variable η, i.e. transverse coordinate.

Lie group analysis of dimensionless transport equations

The group method has been found to be efficient, rigorous and has been successfully implemented in studying an extensive range of engineering fluid dynamics problems [39]. Uddin et al. [40] investigated two-dimensional steady natural convective flow of a nanofluid in a porous medium with group theory. Further chemical flow studies utilizing group theory methods have been reported by Salem and Rania [41], Jalil and Asghar [42] and Rashidi et al. [43]. In the present, we select the following special form of Lie group transformations:

$$\begin{aligned} \Gamma: \quad & x^* = xe^{\varepsilon\alpha_1}, y^* = ye^{\varepsilon\alpha_2}, \psi^* = \psi e^{\varepsilon\alpha_3}, \theta^* = \theta e^{\varepsilon\alpha_4}, \ \phi^* = \phi e^{\varepsilon\alpha_5}, \\ & g^*(x) = g(x)e^{\varepsilon\alpha_6}, l^*_{\ 1}(x) = l_1(x)\, e^{\varepsilon\alpha_7}, l_2^*(x) = l_2(x)e^{\varepsilon\alpha_8}, l_3^*(x) = l_3(x)e^{\varepsilon\alpha_9}. \end{aligned} \tag{12}$$

Here ε is the parameter of the group and $\alpha_i\ (i = 1, 2, 3\cdots, 9)$ are all constants of which at least one is non-zero. Eqns. (8)- (11) will be invariant under the transformations in Eqn. (12) if the $\alpha's$ are connected by:

$$\alpha_2 = -\left(\frac{m-1}{2}\right)\alpha_1, \alpha_3 = \left(\frac{m+1}{2}\right)\alpha_1,\ \alpha_4 = \alpha_5 = 0, \alpha_6 = (1-m)\alpha_1,\ \alpha_7 = (m-1)\alpha_1,$$
$$\alpha_8 = \alpha_9 = -\left(\frac{m-1}{2}\right)\alpha_1 . \tag{13}$$

Following the procedure described in Aziz *et al.* (2012), we have the following invariants:

$$\eta = \sqrt{\frac{(m+1)}{2}}\ y x^{\frac{m-1}{2}},\ \psi = \sqrt{\frac{2}{(m+1)}}\, x^{\frac{m+1}{2}}\ f(\eta),\ \theta = \theta(\eta),\ \phi = \phi(\eta), g(x) = x^{1-m},$$
$$l_1(x) = x^{\frac{1-m}{2}},\ l_2(x) = x^{\frac{1-m}{2}}, l_3(x) = x^{\frac{1-m}{2}}. \tag{14}$$

By virtue of Eqn. (14), the following non-linear ordinary differential boundary layer equations for momentum, energy and species concentration are obtained together with boundary conditions:

$$\left[1 + A(1-\theta)\right] f''' + \left(f - A\theta'\right) f'' - \frac{2m}{(m+1)} f'^2 - \frac{2\Omega}{(m+1)}\left[1 + A(1-\theta)\right] f' - \frac{2M}{(m+1)} f' = 0, \tag{15}$$

$$\left[1 + S\,\theta\right]\theta'' + S\,\theta'^2 + \Pr\left[f\,\theta' - \frac{4m}{(m+1)} f'\theta + Ec\left[1 + A(1-\theta)\right] f''^2 \right] + \frac{2M\ Ec \Pr}{(m+1)} f'^2 = 0, \tag{16}$$

$$(1 + Dc\,\phi)\phi'' + Dc\,\phi'^2 + Sc\left[f\,\phi' - \frac{4m}{(m+1)} f'\phi \right] = 0. \tag{17}$$

subject to the boundary conditions:

$$f(0) = 0,\ f'(0) = 1 + a\left[1 + A\left(1-\theta\right)\right] f''(0), \theta(0) = 1 + b\theta'(0),\ \phi(0) = 1 + d\phi'(0),$$
$$f'(\infty) = \theta(\infty) = \phi(\infty) = 0. \tag{18}$$

Here η is the similarity independent variable and f, θ, ϕ are dimensionless stream function, temperature and concentration. Primes denote derivative with respect to η.

In engineering materials processing and energy systems applications, key quantities of physical interest are the skin friction factor $C_{f\bar{x}}$, local Nusselt number, $Nu_{\bar{x}}$ and local Sherwood number, $Sh_{\bar{x}}$. These are defined, respectively as follows:

$$C_{f\bar{x}} = \frac{\mu(T)}{\rho \bar{u}_w^2(\bar{x})}\left(\frac{\partial \bar{u}}{\partial \bar{y}}\right)_{\bar{y}=0}, Nu_{\bar{x}} = \frac{\bar{x}}{T_w - T_\infty}\left(-\frac{\partial T}{\partial \bar{y}}\right)_{\bar{y}=0}, Sh_{\bar{x}} = \frac{\bar{x}}{C_w - C_\infty}\left(-\frac{\partial C}{\partial \bar{y}}\right)_{\bar{y}=0}. \tag{19}$$

Using Eqs. (7), (14), we have from Eq. (19):

$$\mathrm{Re}_{\bar{x}}^{1/2} C_{f\bar{x}} = \left[1 + A\left(1-\theta\right)\right] f''(0), \mathrm{Re}_{\bar{x}}^{-1/2}\ Nu_{\bar{x}} = -\theta'(0), \mathrm{Re}_{\bar{x}}^{-1/2}\ Sh_{\bar{x}} = -\phi'(0), \tag{20}$$

where $\mathrm{Re}_x = \bar{u}_w\,\bar{x}/\nu$ is the local Reynolds number.

Numerical solutions and validation

The non-linear boundary value problem defined by Eqns. (15)-(17) along with boundary conditions in Eqn. (18) is well-posed and a numerical solution has been obtained using the Runge-Kutta-Fehlberg fourth-fifth order numerical method in **Maple 16**. The step size was assumed to be 0.001 and the convergence criteria was taken as 10^{-6}. The asymptotic boundary conditions, given by Eqn. (20), were replaced by using a value of 15-20 for the similarity variable $\eta_{\max}$ such that $f'(\eta_{\max}) = \theta(\eta_{\max}) = \phi(\eta_{\max}) = 0$**.** The choice of $\eta_{\max}$ ensures that all numerical solutions approached the asymptotic values correctly. In order to verify the accuracy of the present computations, the results of the skin friction factor and the dimensionless heat transfer rates are compared with Yazdi *et al*. [36], Cortell [44] and Chen [45]. For example, our model reduces exactly to the model studied by Yazdi *et* al. [36] for the special case of constant transport properties $(A = S = Dc = 0)$, in non-porous media ($\Omega = 0$ i.e. infinite permeability) and in the absence of thermal slip, solutal slip $(d = 0)$ and viscous and Joule heating (Ec= 0). The comparisons are shown in **Tables 1-4** and an excellent correlation is achieved. This degree of closeness vouches for the high accuracy of the present computational scheme. In **Table 1**, a strong increase in shear stress function (friction factor) accompanies a rise in the power-law index parameter, m. Evidently a strong acceleration in boundary layer flow is achieved with greater non-isothermal and non-isolutal effects, as also computed by Cortell [44]. In **Table 2**, this trend is confirmed by comparison with the results of Yazdi et al. [36] and furthermore in close agreement with Yazdi *et al.* [36], a strong deceleration in the flow is observed with increasing momentum slip factor (a). In **Table 3**, temperature gradient is found to be enhanced with increasing power-law index (m), Reynolds number (Re), Prandtl number (Pr) and also positive Eckert number (Ec), the latter implying greater thermal energy transfer from the wall to the porous medium, with the present solutions corresponding closely to those of Cortell [44]. **In Table 4,** the present shooting solutions (RKF45) for wall heat transfer gradient are compared with the Keller box implicit finite difference solutions of Chen [45]. Three cases are examined. Firstly without viscous heating or Joule (Ohmic) dissipation (Ec = 0). Secondly with viscous heating (the term $PrEc[1+A(1-\theta)f^{//2}]$ is retained in eqn. (16)) but Joule heating is absent (the term $2MEcPr\, f^{/2}/(m+1)$ in eqn. (16) vanishes). Thirdly with both viscous heating i.e. $PrEc[1+A(1-\theta)f^{//2}]$ and Joule heating ($2MEcPr\, f^{/2}/(m+1)$) are retained in Eqn. (16). An increase in Eckert number is observed to slightly decrease heat transfer gradient magnitude for any value of Prandtl or magnetic number. With both Joule and viscous heating present, heat

transfer gradients are lower in value than when these two effects are absent. With increasing Prandtl number there is a significant escalation in heat transfer gradients. An increase in magnetic parameter is found to weakly reduce the heat transfer gradient.

Figs. 2-14 show the effects of the thermo-physical parameters on the flow, heat and mass transfer characteristics. In **Figs 2-4** the response of stream function to a change in inverse permeability parameter, viscosity parameter, magnetic field, thermal slip and momentum slip parameters is illustrated. An increase in viscosity parameter, $A = b_0(T_w - T_\infty)$, significantly increases the stream function magnitudes whereas increasing inverse permeability parameter, $\Omega = \mu_\infty / \rho_\infty K_0 U_r$, decreases stream function (**Fig**. 2). Inspection of **Fig**. 3, indicates that stream function is depressed with increasing thermal slip (*b*) and also magnetic parameter (*M*). **Fig.** 4 shows that a rise in momentum slip (*a*) depresses stream function.

Figs. 5 and 6 show the velocity distributions with variation in several parameters. An increase in viscosity is observed to accelerate the boundary layer flow whereas a rise in inverse permeability parameter causes depression in velocity. In the transformed momentum Eqn. (16), the term -2 Ωf /[1+A(1-θ)] /(m+1), represents the porous medium drag force, based on the Darcy law. This term is directly proportional to Ω, and therefore inversely proportional to permeability of the porous material. Increasing Ω will therefore decrease permeability and this will serve to increase the impedance from porous media fibers to the fluid, thereby decelerating the flow. This is in agreement with the trend shown in **Fig**. 5. Although the viscosity parameter, *A*, arises in several terms in Eqn. (16), the dominant term is that of the highest order, $[1+A(1-\theta)]\, f'''$ and his dominates over other terms. This is an assistive body force and with increasing *A*, this will aid momentum development and accelerate the flow. Fig. 6 shows that with increasing momentum (velocity) slip (*a*) the flow velocity is substantially depressed an effect which is understandably maximized at and near to the wall. Momentum slip is simulated in the wall boundary condition given in Eqn. (18). Increasing momentum slip causes a reduction in the penetration of the stagnant surface through the boundary layer. This serves to reduce the momentum boundary layer thickness since the flow is accelerated. Evidently the presence of momentum slip in real flows has a significant influence near the wall. Without momentum slip ($a = 0$), engineers may underestimate velocities at the wall, and this may adversely affect design calculations. With increasing magnetic field, *M*, the flow is markedly decelerated. The Lorentzian body force arising in the momentum Eqn. (16) is a linear drag force, $-2M f'/(m+1)$. This force retards the boundary layer flow and

increases momentum boundary layer thickness. In the absence of magnetic effects, $M \rightarrow 0$, and the velocity is maximized for this non-conducting scenario. Momentum boundary layer thickness will therefore be minimized in the absence of magnetic field. The strong control of magnetic field on flow even at weak strengths is clearly observed in **Fig.** 6. The pattern observed in **Fig.** 6 for both momentum slip and magnetic field influence concurs with many studies in the literature including Zhang and Zheng [4], Gorla and Hossain [23] etc.

Figs. 7-10 illustrate the temperature distributions in the boundary layer for the effects of permeability, viscosity, thermal conductivity, thermal slip, magnetic field and momentum slip. An increase in viscosity strongly reduces the temperatures in the boundary layer whereas increasing inverse permeability parameter has the opposite effect **(Fig. 7).** The decrease in permeability associated with an increase in Ω, physically implies an increase in the presence of solid fibers in the porous medium. This acts to enhance thermal conduction in the regime and results in heating of the boundary layer regime. **Fig.** 8 indicates that increasing thermal conductivity (*S*) strongly accentuates temperatures. The increase in temperatures with increasing inverse permeability parameter (*Ω)* is confirmed also in this figure. The curvature in profiles is also found to decrease with increasing thermal conductivity and the temperature distribution tends to a linear decay at the highest value of *S***. Fig.** 9 shows that a rise in thermal slip parameter, *b*, which is featured in the boundary conditions (18), markedly decreases temperatures, in particular at the wall. This was observed quite recently by Aziz [46] who also considered a convective boundary condition. Conversely the temperature is significantly elevated with increasing magnetic field effect (M). The Lorentzian hydromagnetic force which enhances the flow causes supplementary work to be expended in dragging the magnetic field. This is distributed as thermal energy and effectively heats the boundary layer regime, elevating temperatures. This is a classical result in magnetohydrodynamic convection and has been identified in many studies including Al-Nimr and Hader [5]. An increase in momentum slip (*a*), as observed in **Fig.** 10, enhances the temperature substantially. The accentuation in velocity and the introduction of greater fluid volumes into the body of the porous medium with increasing momentum slip, serves to heat the regime. Thermal boundary layer thickness is decreased. Greater wall slip velocity is known to increase heat transfer rates from the bounding surface to the fluid as elucidated owing to an increase in advection in a region where diffusion is dominant. The heating effect of the magnetic field (*M*) is again observed in **Fig** 10.

Finally **Figs 11-14** depict the evolution of concentration profiles in the regime with a variation in selected parameters. Increasing viscosity parameter (*A*) is observed to depress concentrations, whereas decreasing permeability (increasing value of Ω), enhances concentration values **(Fig.** 11). Increasing mass diffusivity parameter (*Dc*) strongly elevates species concentration values throughout the boundary layer (**Fig**. 12). Increasing magnetic parameter (M) is found to boost the concentrations whereas an increase in mass slip parameter (d) has the converse effect (**Fig.** 13). An increase in momentum slip (a) however is observed to aid species diffusion and enhances concentration values markedly (**Fig.** 14). In summary the influence of magnetic field, hydrodynamic, thermal and mass slip is significant and further investigations are warranted for more complex studies.

Conclusions

In the present paper we have addressed the influence of viscous and Ohmic dissipation (Joule heating), multiple wall slip phenomena, variable mass diffusivity, variable viscosity, variable thermal conductivity and transverse magnetic field on magneto-thermo-solutal convection in porous media. Numerical solutions have been obtained with **Maple 16** numerical quadrature and validated with a number of studies in the literature. Increasing magnetic field has been observed to enhance temperature and concentration values but to decelerate the flow. An increase in Eckert number enhances temperatures whereas increasing thermal slip effect decreases them. Increasing momentum slip accelerates the flow and heats the boundary layer. Increasing thermal conductivity also elevates temperatures as does a decrease in permeability (increase in inverse permeability parameter). The flow is accelerated with increasing permeability whereas concentration is decreased. An increase in mass diffusivity is shown to elevate species concentrations in the porous medium. The present study has been confined to Newtonian flows. Future investigations will examine non-Newtonian liquids [29] and will be communicated imminently.

REFERENCES

Al-Nimr, M.A., Hader, M.A., 1999. MHD free convection flow in open-ended vertical porous channels. Chem. Eng. Sci. 54, 1883-1889.

Arcos, J.C., Bautista, O., Méndez, F., 2007. Variable viscosity effects on a conjugate laminar film-condensation process. Chem. Eng. Commun. 195, 229-242.

Aziz, A., Lopez, R.J., 2011. Convection-radiation from a continuously moving, variable thermal conductivity sheet or rod undergoing thermal processing. Int. J. Therm. Sci. 50, 1523-1531.

Aziz, A., 2010. Hydrodynamic and thermal slip flow boundary layers over a flat plate with constant heat flux boundary condition. Commun. Nonlinear Sci. Numer. Simul. 15, 573-580.

Azuara, E., Flores, E., Beristain, C.I., 2009. Water diffusion and concentration profiles during osmode hydration and storage of apple tissue. Food Bioprocess Tech. 2, 361–367.

Augier, F., Masbernat ,O., Guiraud, P., 2003. Slip velocity and drag law in a liquid-liquid homogeneous dispersed flow. AIChE J. 49, 2300–2316.

Bég, O.A., Takhar, H.S., Soundalgekar, V.M., Prasad, V., 1998. Thermoconvective flow in a saturated, isotropic, homogeneous porous medium using Brinkman's model: numerical study. Int. J. Numer. Meth. Heat Fluid Flow. 8, 559 – 589.

Bég, O.A., Zueco, J., López-Ochoa, L.M., 2010. Network numerical analysis of optically thick hydromagnetic slip flow from a porous spinning disk with radiation flux, variable thermophysical properties, and surface injection effects. Chem. Eng. Commun. 198, 360-384.

Chen, C.H., 2010. Combined effects of Joule heating and viscous dissipation on magnetohydrodynamic flow past a permeable, stretching surface with free convection and radiative heat transfer. ASME J. Heat Transf. 132, 064503, 5 pages.

Cortell, R.,2012. Heat transfer in a fluid through a porous medium over a permeable stretching surface with thermal radiation and variable thermal conductivity. Canadian J. Chem. Eng. 90, 1347-1355.

Cortell, R., 2008. Effects of viscous dissipation and radiation on thermal boundary layer over a nonlinearly stretching sheet. Phys Letts. A. 372, 631–636.

Cussler, E.L., 2009. Diffusion: Mass Transfer in Fluid Systems, 3rd ed., Cambridge University Press, UK.

Del Casal, E.P., McAvoy, J.J. 1975. Magnetofluid-dynamic separation of a binary gas. AIChE J. 21, 615–618.

Gorla, R.S.R., Hossain, A., 2013. Joule heating effect on magnetohydrodynamic mixed convection boundary layer flow with variable electrical conductivity, Int. J. Numerical Methods Heat Fluid Flow, 23, 10-24.

Hamad, M.A.A., Uddin, M.J., Ismail, A.I.M., 2012. Investigation of combined heat and mass transfer by Lie group analysis with variable diffusivity taking into account hydrodynamic slip and thermal convective boundary conditions. Int. J Heat Mass Transfer. 55, 1355-62.

Muhaimin, I., Kandasamy,R., Hashim, I., 2009. Thermophoresis and chemical reaction effects on non-Darcy MHD mixed convective heat and mass transfer past a porous wedge in the presence of variable stream condition. Proc. IChemE-Chem. Eng. Res. and Des. 87, 1527-1535

Iliuta, I., Larachi, F., 2003a. Magnetohydrodynamics of trickle bed reactors: mechanistic model, experimental validation and simulations. Chem. Eng. Sci. 58, 297-307.

Iliuta, I., Larachi, F. 2003b. Theory of trickle-bed magnetohydrodynamics under magnetic-field gradients. AIChE J. 49, 1525–1532.

Jalil, M., Asghar, S., 2013. Flow of power-law fluid over a stretching surface: A Lie group analysis. Int. J. Non-Linear Mech. 48, 65–71.

Kakimoto, K., Tashiro, A., Ishii, H., Shinozaki, T., 2003. Mechanism of heat and oxygen transfer under electromagnetic CZ crystal growth with cusp-shaped magnetic fields. J. Electrochem. Soc. 150, G648-G652.

Karniadakis, G., Beskok, A., Aluru, N., Microflows and Nanoflows: Fundamentals and Simulation, Springer Science, New York, USA, 2005.

Lok, Y.Y., Pop, I., Ingham, D.B., 2010. Oblique stagnation slip flow of a micropolar fluid. Meccanica 45, 187-198.

Iliuta, I. Grandjean, B.P.A., Larachi, F., 2002. Hydrodynamics of trickle-flow reactors: updated slip functions for the slit models. Proc. IChemE- Chem. Eng. Res. and Des. 80, 195-200.

Mahmoud, M. A. A. 2010. The effects of variable fluid properties on MHD Maxwell fluids over a stretching surface in the presence of heat generation/absorption. Che. Eng. Commun. 198, 131-146.

Mukhopadhyay, S., Layek, G.C., 2012. Effects of variable fluid viscosity on flow past a heated stretching sheet embedded in a porous medium in presence of heat source/sink. Meccanica. 47, 863–876.

Muhaimin, I., Kandasamy, R., Hashim, I., 2010. Scaling transformation for the effects of chemical reaction on free convective heat and mass transfer in the presence of variable stream conditions. Proc. IChemE- Chem. Eng. Res. and Des. 88, 1320-1328.

Rashidi, M. M., Rahimzadeh, N., Ferdows, M., Uddin, M.J., Bég, O.A., 2012. Group theory and differential transform analysis of mixed convective heat and mass transfer from a horizontal surface with chemical reaction effects. Chem. Eng. Commun. 199, 1012-1043.

Rakesh, V., Datta, A.K., Walton, A.H., McCarthy K.L, McCarthy, M.J. 2012. Microwave combination heating: coupled electromagnetics- multiphase porous media modeling and MRI experimentation. AIChE J. 58, 1262–1278.

Rosenbaum, E.E., Hatzikiriakos, S.G., 1997. Wall slip in the capillary flow of molten polymers subject to viscous heating. AIChE J. 43, 598–608.

Salem, A.M., Rania, F., 2012. Effects of variable properties on MHD heat and mass transfer flow near a stagnation point towards a stretching sheet in a porous medium with thermal radiation. Chin. Phys.B. 21, 054701.

Seshadri, R., Na., T.Y.,1985. Group Invariance in Engineering Boundary Value Problems, Springer, New York, USA.

Shateyi, S., Motsa, S.S., 2010**.** Variable viscosity on magnetohydrodynamic fluid flow and heat transfer over an unsteady stretching surface with Hall effect. Boundary Value Probs. 2010, Article ID 257568, 20 pages, **doi:10.1155/2010/257568.**

Su, X., Zheng, L., Zhang, X., Zhang, J., 2012. MHD mixed convective heat transfer over a permeable stretching wedge with thermal radiation and Ohmic heating. Chem. Eng. Sci. 78, 1-8.

Tripathi, D., Pandey, S.K., Siddiqui, A., Bég, O.A., 2012. Non-steady peristaltic propulsion with exponential variable viscosity: a study of transport through the digestive system. Comp. Meth. Biomech. Biomed. Eng. **DOI:10.1080/10255842.2012.703660.**

Tripathi, D., Beg, O.A., Curiel Sosa, J.L., 2012. Homotopy semi-numerical simulation of peristaltic flow of generalized Oldroyd-B fluids with slip effects. Comp. Meth. Biomech. Biomed. Eng. **DOI: 10.1080/10255842.2012.688109 .**

Uddin, M.J., W.A. Khan, A.I. Md. Ismail, Lie group analysis and numerical solutions for magneto-convective slip flow along a moving chemically reacting radiating plate in porous media with variable mass diffusivity, HTAR (Online)

Uddin, M.J., O. Anwar Bég, and N. Amin, Hydromagnetic transport phenomena from A stretching or shrinking nonlinear nanomaterial sheet with Navier slip and convective heating: A model for bio-nano-materials processing. Journal of Magnetism and Magnetic Materials (2014),38, 2014, 252–261.

White, R.E., Subramanian, V.R., 2010. Computational Methods in Chemical Engineering with Maple, New York: Springer.

Woo Inn, Y., 2013. Melt fracture and wall slip of metallocene-catalyzed bimodal polyethylenes in capillary flow. J. Rheol. 57, 393-406.

Ybarra, R.M., Eckert, R.C. 1980. Viscous heat generation in slit flow. AIChE J. 26, 5, 751–762

Yacob, N.A., Ishak, A., 2011. MHD flow of a micropolar fluid towards a vertical permeable plate with prescribed surface heat flux. Proc. IChemE-Chem. Eng. Res. and Des. 89, 2291-2297.

Zhang, Y., Zheng, L., 2012. Analysis of MHD thermosolutal Marangoni convection with the heat generation and a first-order chemical reaction. Chem. Eng. Sci. 69, 449-455.

Yazdi, M.H., Abdullah, S., Hashim, I., Sopian, K. 2011. Slip MHD liquid flow and heat transfer over non-linear permeable stretching surface with chemical reaction. Int. J. Heat and Mass Transf. 54, 3214–3225.

Zueco, J. Bég, O.A., 2011. Network numerical simulation of hydromagnetic marangoni mixed convection boundary layer. Chem. Eng. Commun. 198, 552-571.
Zueco, J., Bég, O.A., Takhar, H.S., Prasad, V.R., 2009. Thermophoretic hydromagnetic dissipative heat and mass transfer with lateral mass flux, heat source, Ohmic heating and thermal conductivity effects: Network simulation numerical study. Appl. Thermal. Eng. 29, 2808-2815.

Figure Captions

1. Physical model and coordinate system.
2. Effect of permeability and viscosity variation on stream function
3. Effect of magnetic field and thermal slip on stream function
4. Effect of magnetic field and velocity slip on stream function
5. Effect of permeability and viscosity variation on velocity.
6. Effect of velocity slip and magnetic field on velocity.
7. Effect of permeability and viscosity variation on temperature
8. Effect of permeability and thermal conductivity on temperature
9. Effect of thermal slip and magnetic field on temperature
10. Effect of velocity slip and magnetic field on temperature
11. Effect of permeability and viscosity variation on concentration
12. Effect of permeability and mass diffusivity parameter on concentration
13. Effect of mass slip and magnetic field on concentration
14. Effect of velocity slip and magnetic field on concentration

Table Captions

1. Comparison of the skin friction results for $a = b = d = A = S = \Omega = Ec = 0$.

2. Comparison of skin friction, $-f''(0)$ for $b = d = A = S = Ec = M = \Omega = 0$.
3. Comparison of temperature gradients for $a = b = d = A = S = M = \Omega = 0$.
4. Comparison of heat transfer rates for Pr, M and Ec: $a = b = d = A = S = \Omega = 0, m = 1$

Figures

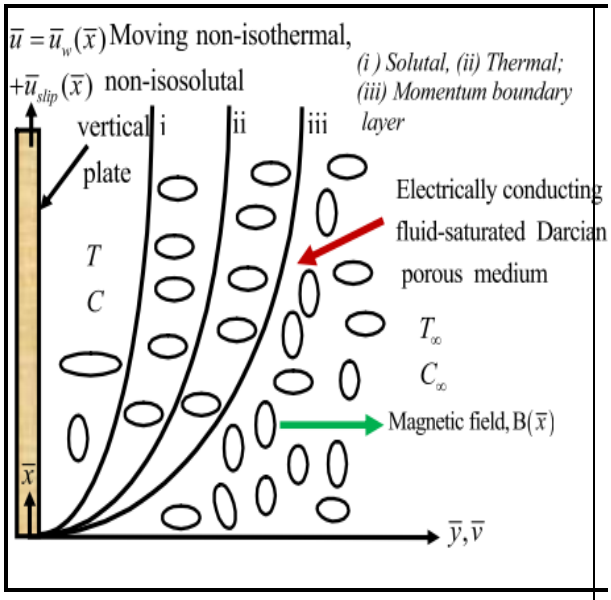

Fig.1

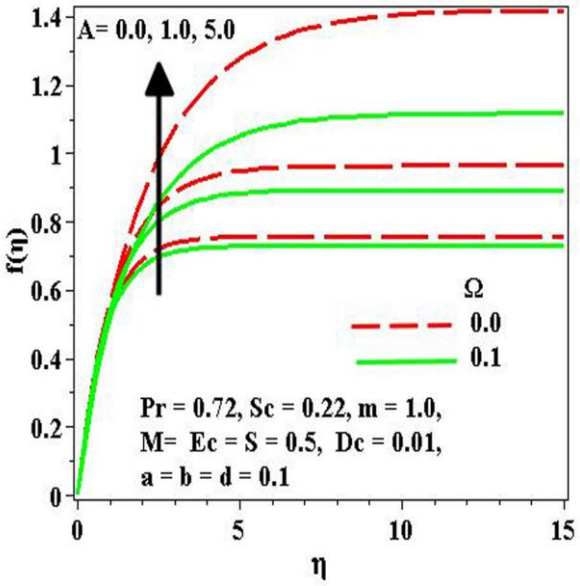

Fig.2

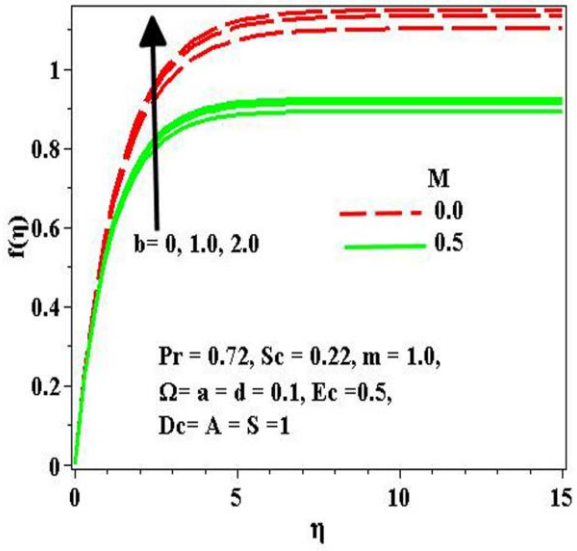

Fig.3

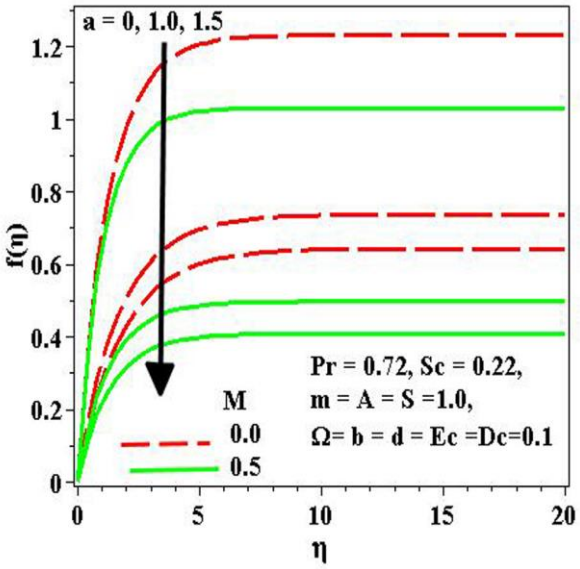

Fig.4

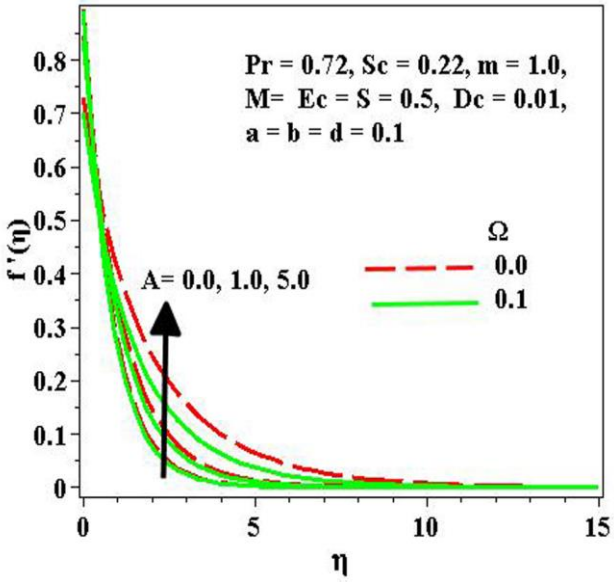

Fig.5

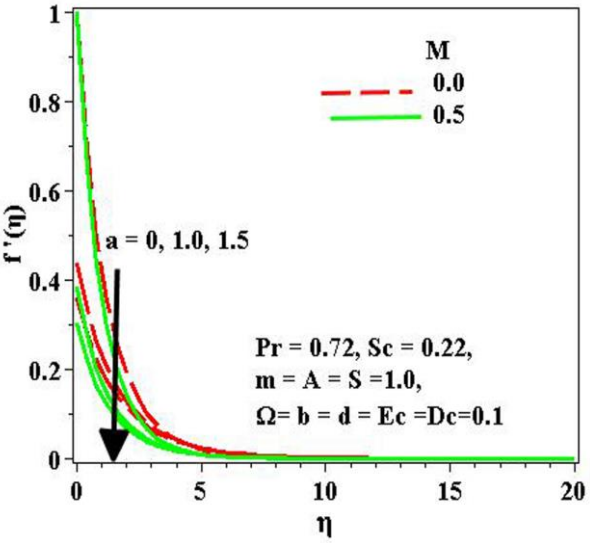

Fig.6

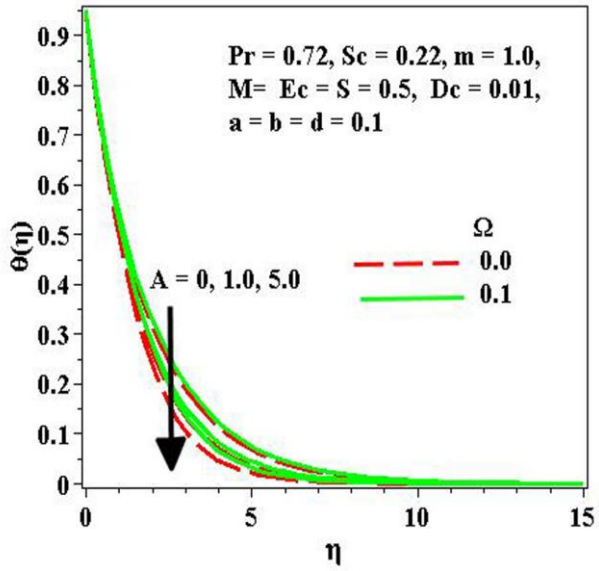

Fig.7

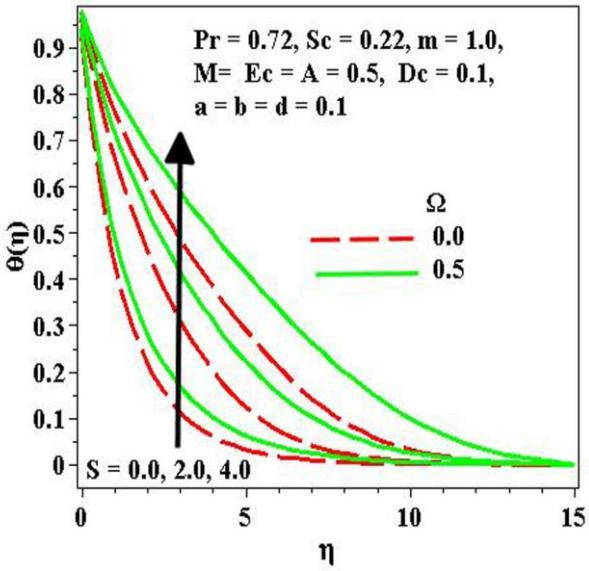

Fig.8

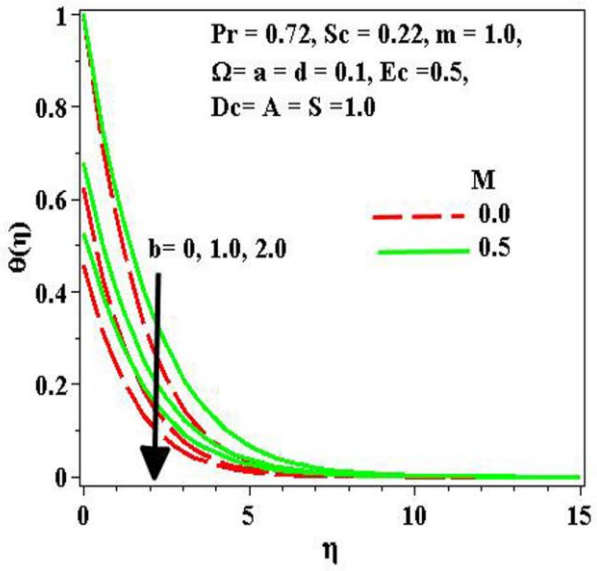

Fig.9

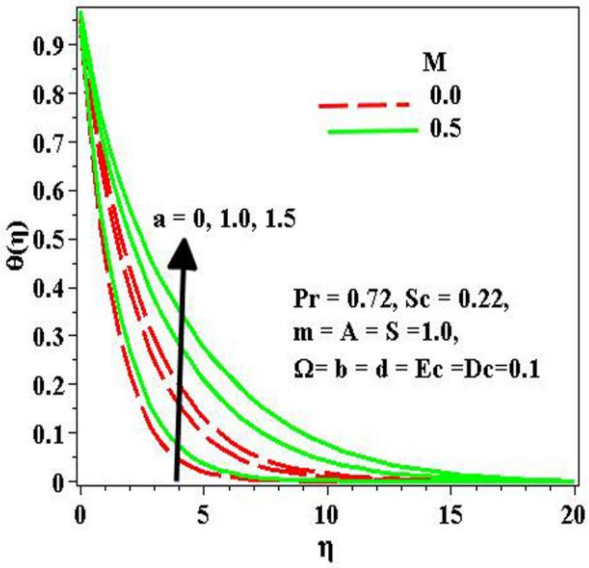

Fig.10

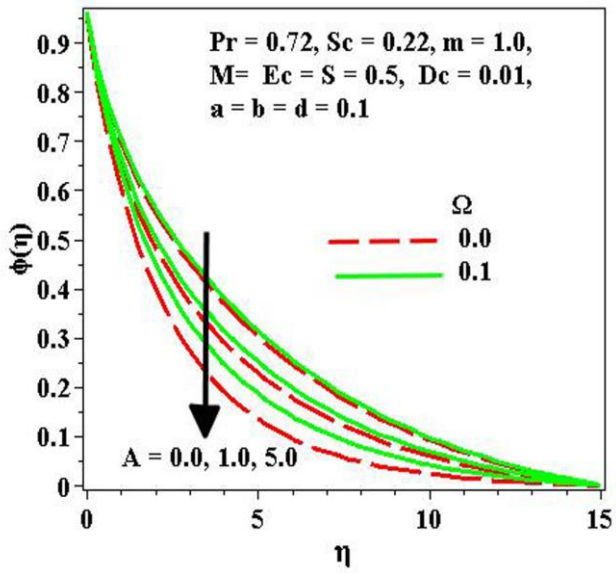

Fig.11

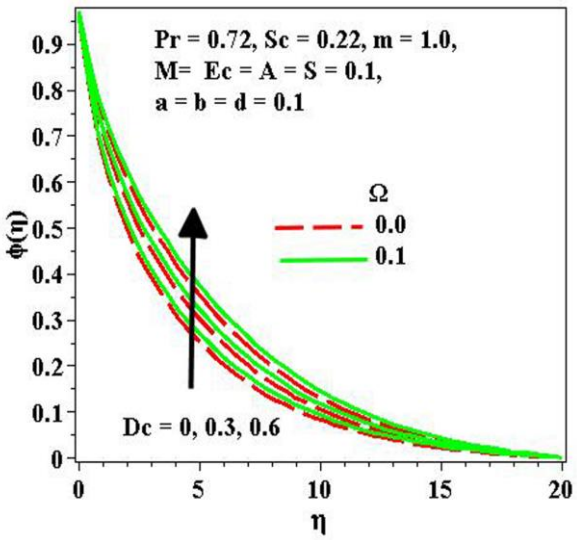

Fig.12

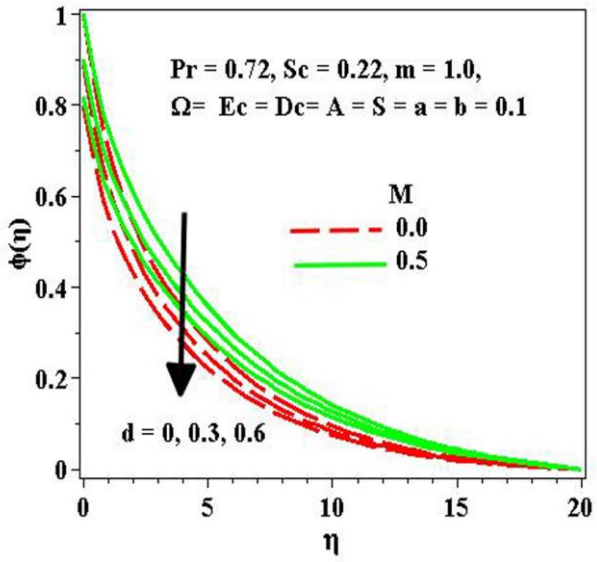
Pr = 0.72, Sc = 0.22, m = 1.0,
Ω= Ec = Dc= A = S = a = b = 0.1
M
0.0
0.5
d = 0, 0.3, 0.6
Φ(η)
η

Fig.13

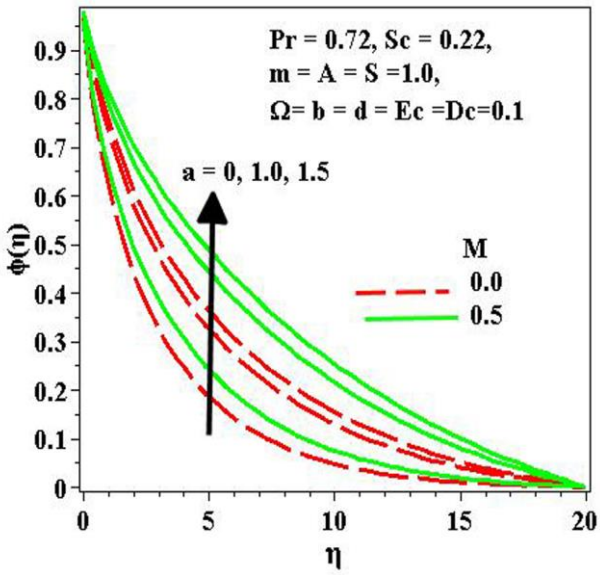
Pr = 0.72, Sc = 0.22,
m = A = S =1.0,
Ω= b = d = Ec =Dc=0.1
a = 0, 1.0, 1.5
M
0.0
0.5
Φ(η)
η

Fig.14

Tables

Table 1

m	$-f''(0)$	
	Cortell [44]	Present
0.1	0.70590	0.70592
0.3	0.81570	0.81571
0.6	0.91817	0.91818
0.9	0.98324	0.98325
1	1.00000	1.00000
1.5	1.06159	1.06160
3	1.14859	1.14859
10	1.23488	1.23488

Table 2

m	a	Yazdi et al. [36]	Present
0	0	0.6275	0.62755
0.2		0.7667	0.76684
0.5		0.8896	0.88954
0.75		0.954	0.95396
1		1	1.00002
	0.5	0.5912	0.59120
	1	0.4302	0.43016
	2	0.284	0.28398

Table 3

				$-\theta'(0)$	
m	Pr	Re	Ec	Cortell [44]	Present
1.5	1	1	0.1	0.82336	0.82891
3				0.91377	0.91422
10				1.00157	1.00243
1.5	2			1.28058	1.28065
	5			2.17878	2.17884
	2	2		1.56499	1.56577
		5		1.83389	1.84578
		1	0.5	1.15954	1.15959

Table 4

			$-\theta'(0)$					
			No Joule heating *or* viscous dissipation		No Joule heating but with viscous dissipation		With Joule heating *and* viscous dissipation	
Pr	*M*	*Ec*	Chen[45] Kellerbox	Present RKF45	Chen [45] Keller box	Present RKF45	Chen [45] Keller box	Present RKF45
1	1	0.0	1.215774	1.215778				
		0.05			1.188896	1.188899	1.175457	1.175461
		0.1			1.162018	1.162022	1.135141	1.135145
	2	0.0	1.126901	1.1269004				
		0.05			1.091843	1.091842	1.068471	1.068470
		0.1			1.056785	1.056784	1.010041	1.0100403
10	1	0.0	4.690210	4.69021450				
		0.05			4.535061	4.53506554	4.457487	4.45749107
		0.1			4.379912	4.37991658	4.22476764	4.224767632
	2	0.0	4.606911	4.60691406				
		0.05			4.392634	4.39263673	4.249783	4.2497851744
		0.1			4.178357	4.17835939	3.892654	3.8926562839
100	1	0.0	15.609144	15.6092254				
		0.05			14.943482	14.9435588	14.610650	14.610725550
		0.1			14.277819	14.2778922	13.612157	13.612225633
	2	0.0	15.529686	15.5299946				